Spectrochimica Acta Part A: Molecular and Biomolecular Spectroscopy 224 (2020) 117450

Contents lists available at ScienceDirect

Spectrochimica Acta Part A: Molecular and Biomolecular Spectroscopy

journal homepage: www.elsevier.com/locate/saa

Study on fluorescence spectroscopy of PAHs with different molecular structures using laser-induced fluorescence (LIF) measurement and TD-DFT calculation

Yiran Zhang [a], Peng Liu [b], Youping Li [a], Reggie Zhan [a], Zhen Huang [a], He Lin [a,*]

[a] Key Laboratory for Power Machinery and Engineering of Ministry of Education, School of Mechanical Engineering, Shanghai Jiao Tong University, Shanghai 200240, China

[b] King Abdullah University of Science and Technology (KAUST), Clean Combustion Research Center, Thuwal 23955-6900, Saudi Arabia

ARTICLE INFO

Article history:
Received 8 July 2019
Received in revised form
2 August 2019
Accepted 3 August 2019
Available online 5 August 2019

Keywords:
Laser-induced fluorescence (LIF) spectra
Polycyclic aromatic hydrocarbons (PAHs)
Molecular structures
Aliphatic branched chains
TD-DFT calculation
Electronic emission characteristics
HOMO and LUMO

ABSTRACT

Laser-induced fluorescence (LIF) is an effective technique for non-intrusive and on-line measurement of PAHs in sooting flames but it is still need further investigation due to the complexity of PAH fluorescence characteristics. Therefore, in-depth investigations on the fluorescence spectroscopy of PAHs with different molecular structures are relevant. In this study, we investigated the fluorescence spectrum characteristics of 13 gas-phase PAHs using LIF measurement and time-dependent density functional theory (TD-DFT) calculation. The experimental results showed that the fluorescence emission wavelengths increased with more aromatic (benzenoid) rings, but this relationship no longer existed when the PAH molecules contain the five-membered ring structures. The TD-DFT calculation showed that the fluorescence emission wavelength ranges of PAHs with different molecular structures were dominantly determined by the electronic structures of highest occupied molecular orbital (HOMO) and lowest unoccupied molecular orbital (LUMO) and their energy gaps. It was found that the saturated aliphatic branched chains (methyl and ethyl) only slightly influenced the LIF spectra, while the unsaturated aliphatic branched chains (ethenyl and ethynyl) caused remarkable redshifts. The TD-DFT results indicated that the aliphatic branched chains changed the electric structures of HOMO and LUMO of the core aromatic rings, and then influence the fluorescence emission wavelength ranges.

1. Introduction

Polycyclic aromatic hydrocarbons (PAHs) catch a lot of attention in many research areas, such as combustion [1–7], environmental and biology science [8–10], astrochemistry [11,12] and materials science [13,14]. PAHs are mainly generated from the incomplete combustion of hydrocarbon fuels and are considered to be the main processors of soot particles [15–19]. Extensive studies have concentrated on the PAH and soot formation mechanisms [20–25]. However, understanding of PAH and soot formation, especially the nucleation process of nascent soot particles, still has long-standing challenges [26,27]. The accurate and reliable diagnostic method for the PAH information is crucial to better understand the formation process of PAHs and soot in flames. Laser-induced fluorescence (LIF) is a widely used technique for non-intrusive and on-line measurement of PAHs in various sooting flames [25]. The fluorescence emission wavelengths of PAHs are generally increased with the molecular sizes, so the relative size classes of PAHs can be distinguished approximatively by using different detection wavelength bands in the LIF measurement [28–32]. However, it is still challenging to distinguish the specific PAH species using the existing LIF technique, due to the complexity of PAH fluorescence characteristics and the absence of fluorescence spectrum data [33,34]. Despite these limitations, in situ measurements by optical methods, such as LIF technique, are the only option to obtain PAH information in unfriendly conditions such as turbulent flames [33].

Numerous works have been conducted to obtain the fluorescence spectrum data of PAHs in recent years. F. Ossler et al. [35,36] measured the LIF spectra of gas-phase naphthalene, fluorene, anthracene, and pyrene in an optical cell using 266 nm for excitation. Z. Chi et al. [37,38] detected the fluorescence spectra of anthracene, phenanthrene, pyrene and chrysene vapors in a heated optical cell with the excitation wavelength of 337 nm. Our group [39,40] experimentally investigated the LIF spectrum characteristics of naphthalene, phenanthrene, pyrene, fluorene and fluoranthene and their mixtures in an optical cell at a wide temperature range. All these LIF spectrum data detected in gas-phase revealed that PAHs have somewhat complicated molecular structures and thus emit broad and complex fluorescence spectra that overlap

* Corresponding author.
E-mail address: linhe@sjtu.edu.cn (H. Lin).

https://doi.org/10.1016/j.saa.2019.117450
1386-1425/

with each other. This kind of spectrum overlap will make PAH diagnosis difficult in flames. The molecular structures have a clear influence on the fluorescence spectroscopy of PAHs, therefore, in-depth investigations on the fluorescence spectroscopy of PAHs with different molecular structures are of concern.

The LIF spectrum of PAHs with different molecular size classes (number of benzenoid rings) have been investigated extensively, since these PAHs are the most abundant aromatic species in sooting flames [33]. Even so, the influences of the number of benzenoid rings on the LIF spectra are still not well explained in the level of the molecular structures theoretically. Recent studies suggest that PAHs with five-membered ring structures formed following hydrogen abstraction - C_2H_2 addition (HACA) mechanism [3] are also abundant in sooting flames and play a key role in PAH growth and soot nucleation [41,42]. The spectrum characteristics of other PAH with five-membered ring structures need to be investigated. In addition, PAHs with aliphatic branched chains are widely detected in nascent soot and are proved to be important intermediates for the nucleation of soot particles [17,43–50], however, the spectrum characteristics of these PAHs are not considered in previous studies.

To illuminate the influences of molecular structure on LIF spectrum, quantum chemistry calculation is a kind of essential method. The time-dependent density functional theory (TD-DFT) combined with Franck-Condon approximation is a particularly well-suited method to calculate the vibrationally-resolved electronic absorption and emission spectra of PAHs [51–53]. TD-DFT is capable of calculating the transition energies to the low-lying excited states of PAHs and the standard deviation compared with experimental results is within 0.3 eV [53–55]. Therefore, this theoretical quantum chemistry TD-DFT method has the potential to interpret the LIF spectrum characteristics, and to predict the fluorescence spectra of PAHs when the pure standards are unavailable [56,57].

This study aims to find the influences of PAHs structures, including different molecular size classes, five-membered ring structures, and aliphatic branched chains, on fluorescence characteristics in molecular level. Considering this, in the present study, the fluorescence spectrum characteristics of 13 typical gas-phase PAHs with different molecular structures were systematically investigated using LIF measurement and TD-DFT calculation. These PAHs are extensively formed in sooting flames, and are identified as the interesting targets for in-flame LIF measurement. In the LIF measurement, the LIF spectra of each aforesaid PAH were measured in an optical cell. In TD-DFT calculation, the vibrationally-resolved electronic emission spectra were calculated using the combination of TD-DFT method and Franck-Condon approximation. Then, we calculate the vertical emission energy, electron transition characteristics, and frontier molecular orbitals, with them to explore the mechanisms of PAHs molecular structure determining their fluorescence spectrum characteristics.

2. Methodology

2.1. Experimental methods

The LIF measurement system used in this study consisted of a PAH gasification system, an optical cell, and a LIF diagnostic system, as shown in Fig. 1. This experimental system is identical to the one used in our previous studies [39,40], and is only described here briefly. Using the PAH gasification system, the solid-state commercial PAH standards can be gasified to homogeneous gas phase under argon atmosphere and then conveyed to the optical cell for LIF measurement. The optical cell had three quartz optical windows for laser propagation and fluorescence detection, and the temperature in the optical cell can be controlled by a tube furnace at

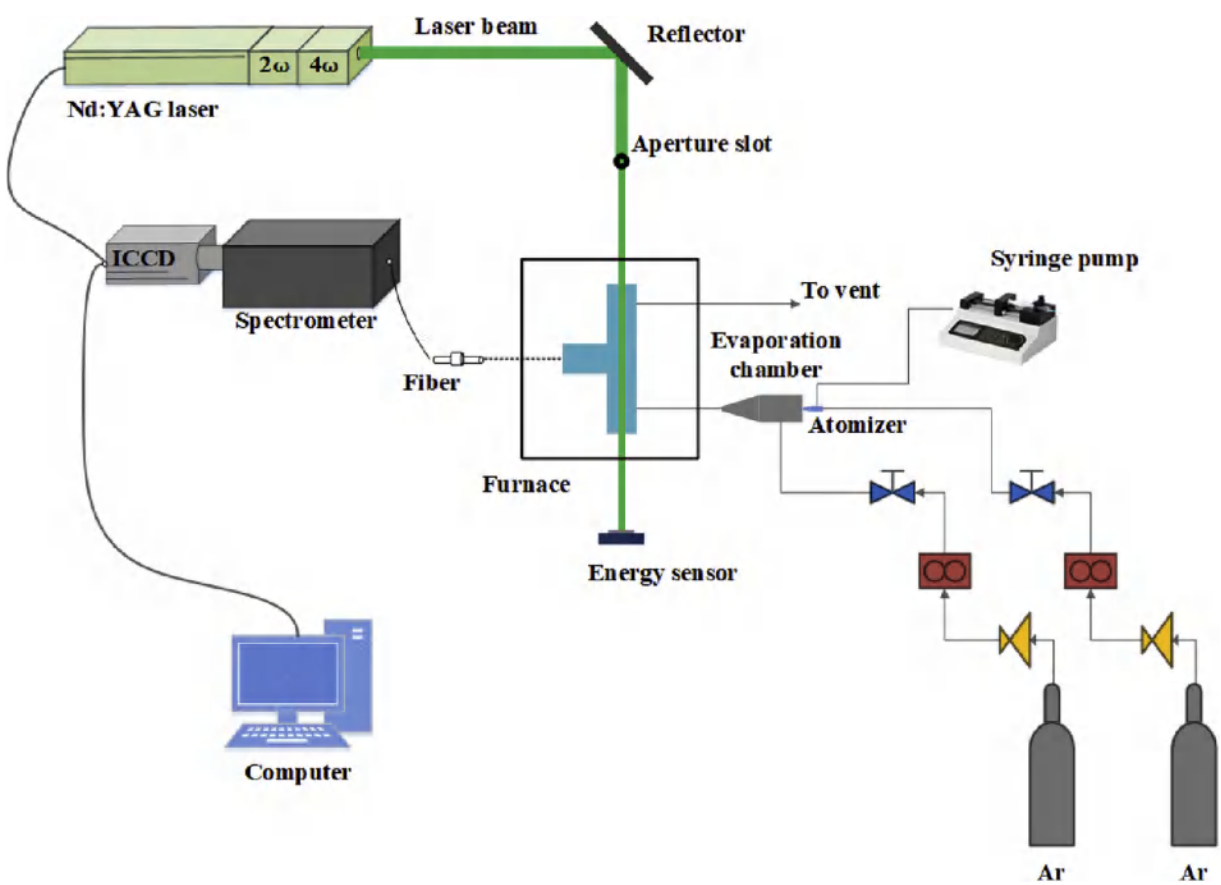

Fig. 1. Schematic of experimental setup.

673−1373 K. The experiments were conducted at 0.1 MPa. The mole fractions of these PAHs were all fixed at 2×10^{-5} throughout the experiments, which were close to the PAH mole fractions in flame conditions. The LIF diagnostic system mainly contained an excitation light source and detection system. The excitation light was supplied by the fourth harmonic (266 nm) of a pulsed Nd:YAG laser (Quantel Q-smart 850). The central portion of the laser beam firstly passed through a 4-mm aperture slot and then directed to the fluorescence probe region. The fluorescence signals were captured by an optical fiber placed at a right angle with respect to the laser propagation and conveyed to a spectrometer (Princeton SP-2-500i). An intensified charge-coupled device (ICCD, Princeton PIMAX3) camera connected at the exit of the spectrometer was used to record the fluorescence signals. The parameters of the detection system were also the same as those in our previous papers [39,40].

2.2. Chemicals and materials

The commercial PAH standards were all purchased from suppliers and used without further purification. The molecular structures of these investigated PAHs were listed in Fig. 2. Naphthalene, phenanthrene, and pyrene containing two, three and four aromatic rings respectively, were selected to study the influence of the number of aromatic rings. Anthracene and naphthacene have three and four aromatic rings respectively, but the enthalpies of formation for these kinds of acenes (linear PAHs) are much higher than those of the peri-condensed PAHs of comparable sizes (phenanthrene and pyrene). Therefore, anthracene and naphthacene are almost not detected in flames [21,58,59] and were not considered in this study. Acenaphthylene, fluorene, and fluoranthene were the most abundant PAHs containing five-membered ring structures in sooting flames. Acenaphthene was selected to do a comparative study with acenaphthylene and to check the effect of PAH hydrogenation on its fluorescence characteristics. To analyze the influence of substituted branched chains, naphthalene (A_2) was chosen as a representative PAH, and the investigated substituted groups were methyl (1-methyl-A_2, 2-methyl-A_2, 1,3-dimethyl-A_2), ethyl (1-ethyl-A_2), ethenyl (2-ethenyl-A_2) and ethynyl (2-ethynyl-A_2).

2.3. TD-DFT calculation methods

On the basis of the Kasha's rule [60], the photon emission of an excited molecule occurs in appreciable yield only from the lowest excited state of a given multiplicity, therefore, only the electron transition between the ground state (S_0) and the first excited state (S_1) was considered in this study. The S_0 and S_1 calculations were carried out using the combination of DFT and TD-DFT methods, with B3LYP exchange-correlation functional and 6−31 + G (d, p) basis set [61,62]. The B3LYP functional has been proven to give accurate results for the S_0 properties and the energy between the HOMO and LUMO orbitals [57].

A three-step procedure [63,64] was used to calculate the vibrationally-resolved electronic spectra in Gaussian 09 program package [65]. Firstly, the S_0 geometries of the investigated PAHs were optimized, and the vibrational frequency analyses were conducted to confirm that all of the optimized geometries were in minimum energy. The molecular structures shown in Fig. 2 were the optimized structures at S_0. Secondly, the S_1 geometries were optimized based on the optimized S_0 structures, in the same way, the frequency analyses were also performed to confirm the minimum energy of the optimized geometries. It should be noted that the S_1 optimization might obtain imaginary frequency if its S_0 geometry has a plane of

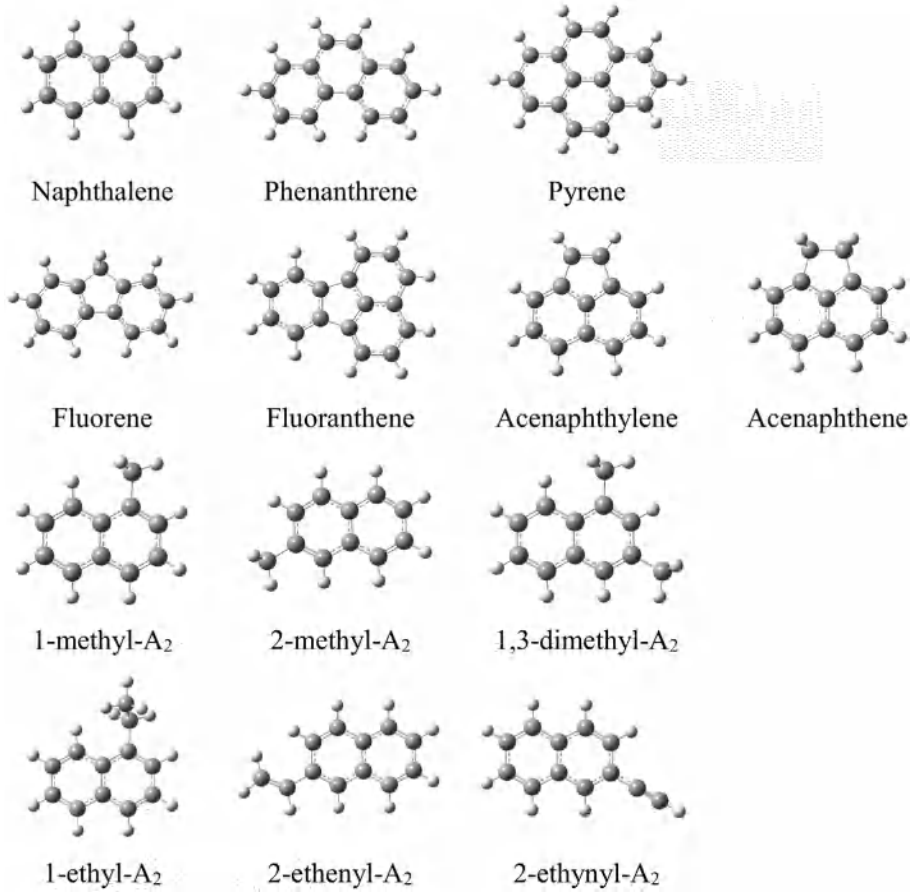

Fig. 2. Molecular structures of the investigated PAHs (A_2 is the abbreviation of naphthalene).

symmetry due to the difference of symmetry between the ground and excited states [53,55]. So, the symmetry of the S_0 structure was broken slightly in S_1 optimization process. In these two steps, geometric coordinates, vertical emission energy, energies of frontier molecular orbitals, electron transition characteristics, and vibrational frequencies of S_0 and S_1 can be obtained. Thirdly, based on results of the frequency calculation at S_0 and S_1, the calculation of Franck-Condon integral was conducted to obtain the vibrationally-resolved emission spectra. To simulate the spectrum shapes of PAHs, the stick-spectrum should be convoluted using a Gaussian function with an appropriate half-width at the half-maximum (HwHm, 135 cm^{-1} by default) [61]. For the investigated PAHs, the HwHm was adjusted to better reproduce the broad structure of the experimental spectrum and 500 cm^{-1} was finally chosen in this study.

3. Results and discussion

3.1. PAHs with different molecular size classes

In this section, the fluorescence spectra of seven gas-phase PAHs including naphthalene, phenanthrene, pyrene, fluorene, fluoranthene, acenaphthylene, and acenaphthene were measured using LIF technique. Naphthalene, phenanthrene, and pyrene have two, three and four benzenoid rings, respectively. The structures of fluorene, fluoranthene, acenaphthylene, and acenaphthene contain a five-membered ring. In this way, the influences of the molecular size classes and five-membered ring structures on the fluorescence characteristics can be analyzed.

3.1.1. Experimental results

The measured LIF spectra of six gas-phase PAHs at 673 K were normalized by their own maximum values as shown in Fig. 3. However, the LIF spectrum of acenaphthylene was not detected in this experiment. This is an interesting phenomenon that the fluorescence intensity from acenaphthylene is too weak to be detected in spite of its structural similarity to naphthalene and acenaphthene. From the literature, it can be concluded that and the quantum efficiency of acenaphthylene for UV excitation is quite low [18,66,67]. In addition, the fluorescence lifetime of acenaphthylene, which was reported in the literature [68,69], was less than 1 ns. Therefore, the fluorescence signal of acenaphthylene could not be captured in this nanosecond LIF system.

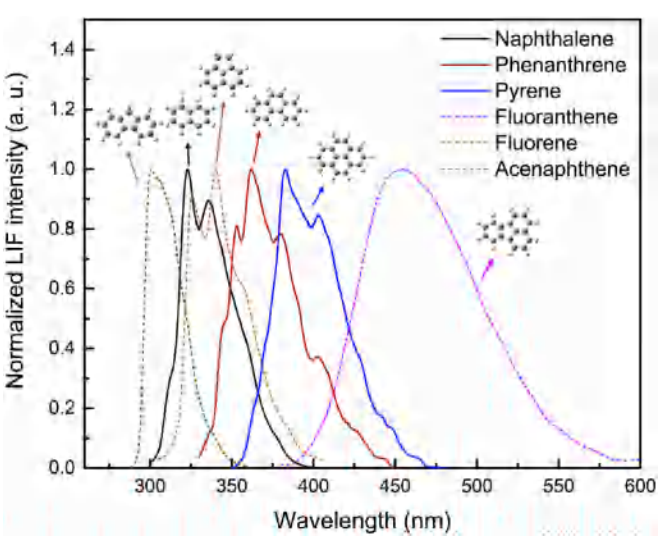

Fig. 3. Experimental LIF spectra of six gas-phase PAHs with different molecular size classes (solid lines) and five-membered ring structures (dashed line) at 673 K and 1 atm in argon. (The data of naphthalene, phenanthrene, pyrene, fluorene and fluoranthene were cited from our previous paper [39].)

It can be observed from the LIF spectra of naphthalene, phenanthrene and pyrene (shown in solid lines) in Fig. 3 that their fluorescence emission wavelengths increase with more aromatic (benzenoid) rings, i.e. larger molecular size. But the fluorescence emission wavelengths of PAHs with five-membered ring structures (shown in dashed line in Fig. 3) no longer increase with increasing number of rings (or larger molecular size), indicating that the emission wavelengths of PAHs are significantly sensitive to the five-membered ring structures. As shown in Fig. 2, acenaphthene and acenaphthylene have very similar molecular structures (the only difference is a single band or double band in their five-membered rings), but their fluorescence properties are totally different. The LIF spectrum shape of acenaphthene is mainly within UV region, and is very similar to that of naphthalene and only red shifted around 5 nm (at the half-maximum position). But the LIF spectrum of acenaphthylene could not be observed in this experiment. Phenanthrene and fluorene both have three rings and similar structures, but the emission wavelengths of fluorene are much shorter than those of phenanthrene and even shorter than those of naphthalene which only has two rings. Pyrene and fluoranthene both have four rings, but the emission wavelengths of fluoranthene are much longer than those of pyrene. To sum up, caution should be taken to distinguish the relative size classes of PAHs according to the relationship of the fluorescence emission wavelength and molecular structures.

To compare the LIF spectra shape of different PAHs, the measured LIF spectra in Fig. 3 were normalized by their own maximum values. In addition, the relative intensities among different PAHs are essential information to analyze the LIF spectra measured in flames containing many different PAHs. Therefore, the normalization factors of the experimental LIF spectra of six gas-phase PAHs in Fig. 3 were listed in Table 1, when the value of naphthalene is set as 1.

3.1.2. Comparison of experimental and calculated LIF spectra

In this section, the experimental and the calculated LIF spectra were compared to confirm the reliability of TD-DFT calculation. The experimental LIF spectrum of acenaphthylene, which could not be detected by the nanosecond LIF system used in this study, was obtained on picosecond laser excitation (355 nm) of a cyclohexane solution at room temperature (cited from the literature [69]). This indicates that the excitation wavelength will influence the LIF spectra of PAHs, and the effect of excitation wavelength have been investigated by S. Bejaoui et al. [70]. The experimental and the calculated LIF spectra were normalized by their own maximum values, as shown in Fig. 4. We observed that the spectrum shape and the position of characteristic peaks were accurately predicted by TD-DFT calculation. On the other hand, the deviations of the emission wavelengths between the experimental and the calculated spectra at the half-maximum position were noted in Fig. 4. The calculated emission spectra of naphthalene, pyrene, fluorene, fluoranthene, and acenaphthene match well with the measured spectra. Compared with the experimental results, the calculated spectra of phenanthrene were narrower, while the calculated spectrum of acenaphthylene was broader and red shifted. The deviations may be caused by the temperature effects because the LIF spectra of gas-phase PAHs (except acenaphthylene) were measured at 673 K in the optical cell while the vibrationally resolved electronic spectra were calculated at 0 K using TD-DFT method. The temperature effect cannot be considered in TD-DFT calculation, but our previous results [39] showed that the spectra of PAHs shift to the red and become broader as temperature increased, and the variation is independent on PAHs structure and size. The temperature dependences of integral fluorescence intensities and normalized fluorescence spectra with temperatures in the range of 673−1373 K can be found in our previous paper [39] but not shown here due to the space limitation.

Table 1
Normalization factors of the experimental LIF spectra of six gas-phase PAHs with different molecular size classes.

Species	Naphthalene	Phenanthrene	Pyrene	Fluorene	Fluoranthene	Acenaphthene
Factor	1	0.705	1.933	2.158	1.068	2.443

3.1.3. Discussion based on the TD-DFT calculation

According to Kasha's rule, the electrons at high excited states will rapidly redistribute to S_1, then the electrons at S_1 will go back to S_0 and emit fluorescence. The electron transition process from S_1 to S_0 was investigated to analyze the fluorescence characteristics of PAHs based on the TD-DFT calculation. The vertical emission energy of S_1 state and $S_0 \rightarrow S_1$ transition nature of seven gas-phase PAHs were listed in Table 2. The rank of the calculated vertical emission energy (at wavelength) was in the following order: fluorene (301.83) < naphthalene (324.34) < acenaphthene (335.41) < phenanthrene (369.72) < pyrene (378.39) < fluoranthene (473.56) < acenaphthylene (608.83), which was in accordance with the order of their experimental fluorescence wavelengths. The calculated transition natures indicated that for these investigated PAHs except phenanthrene, the H → L transition dominantly contributed to the $S_0 \rightarrow S_1$ transition, where H denotes HOMO and L donates LUMO.

In consequence, to interpret the electronic transition properties of PAHs with different molecular structures, the energy gaps (ΔE_{H-L}) between HOMO and LUMO and the electronic structures of HOMO and LUMO were calculated, as shown in Fig. 5. In this study, the ΔE_{H-L} was defined as the difference in energy between HOMO at S_0 state and the LUMO at S_1 state, which was the same as the definition in the literature [71,72]. The rank of the ΔE_{H-L} for these PAHs except phenanthrene was identical with the rank of their experimental and calculated fluorescence wavelengths. For the

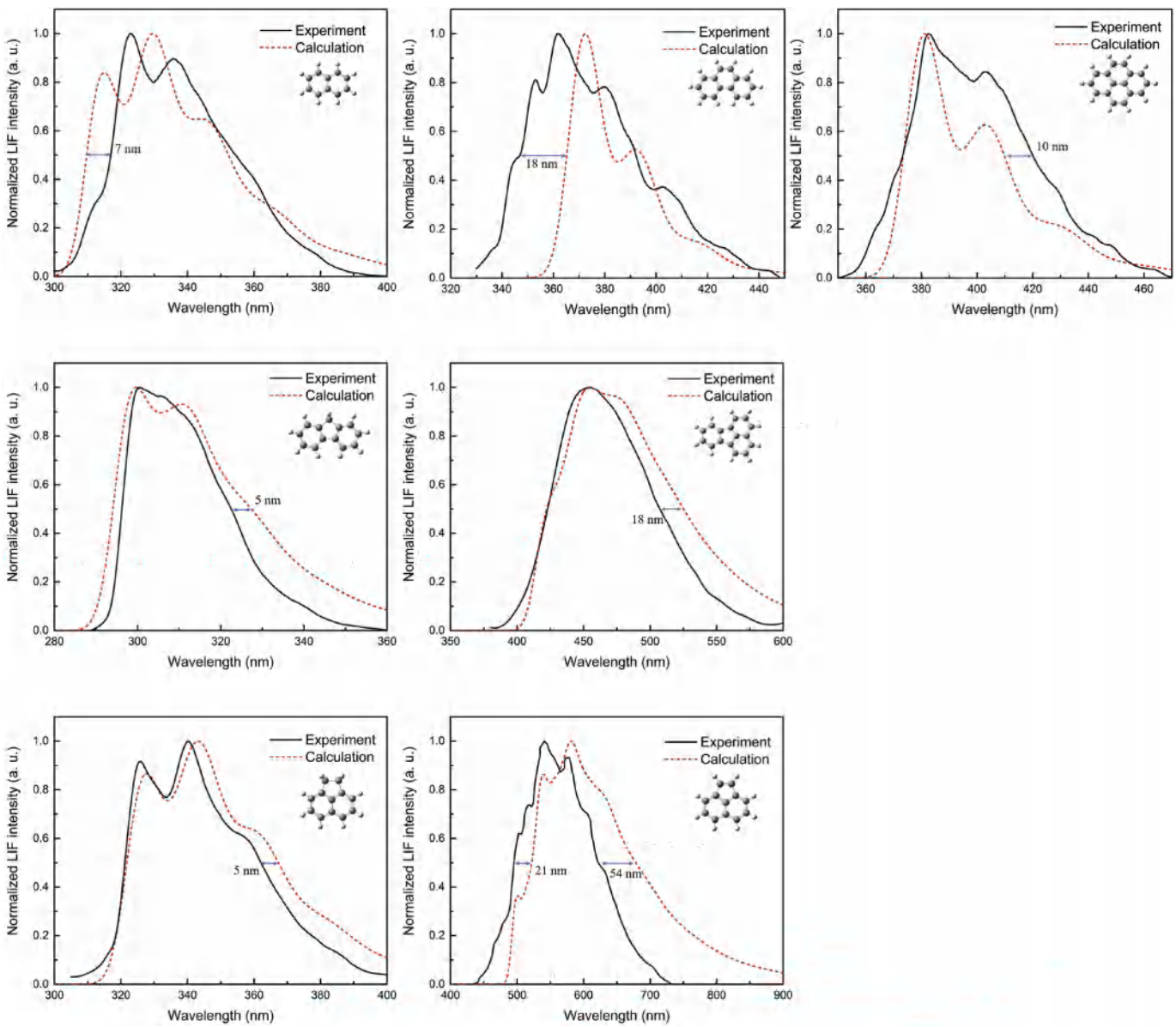

Fig. 4. Comparison of the experimental (black solid line) and calculated (red dashed line) LIF spectra of seven gas-phase PAHs with different molecular size classes. (The experimental data of acenaphthylene were cited from the literature [69].)

Table 2
Electronic transition properties of seven gas-phase PAHs with different molecular size classes.

Species	Vertical emission energy of S_1 state (eV, nm)	$S_0 \rightarrow S_1$ transition nature
Naphthalene	3.8227 (324.34)	H → L (96.8%)
Phenanthrene	3.3534 (369.72)	H → L + 1 (64.7%) H − 1 → L (35.2%)
Pyrene	3.2766 (378.39)	H → L (96.0%)
Fluoranthene	2.6181 (473.56)	H → L (97.9%)
Fluorene	4.1078 (301.83)	H → L (93.6%)
Acenaphthylene	2.0364 (608.83)	H → L (97.9%)
Acenaphthene	3.6965 (335.41)	H → L (97.2%)

PAHs whose $S_0 \rightarrow S_1$ transitions were dominantly contributed from H → L transition, a larger ΔE_{H-L} means that electrons at S_0 state need more energy to jump to S_1 state. Correspondingly, the fluorescence emitted from $S_1 \rightarrow S_0$ transitions have larger vertical emission energy (smaller emission wavelength). Phenanthrene whose $S_0 \rightarrow S_1$ transition was heavily contributed from H → L + 1 and H − 1 → L, the ΔE_{H-L} cannot explain its rank of fluorescence wavelength. It can be seen from Fig. 5 that the electronic structures (electron density plots) of HOMO and LUMO were significantly influenced by the molecular structures of PAHs. Consequently, the PAHs with different molecular structures have different ΔE_{H-L}, which determine their fluorescence emission wavelength range.

3.2. PAHs with aliphatic branched chains

In this section, we explored the effects of aliphatic branched chains substituted at naphthalene (A_2) molecule on the fluorescence characteristics. The LIF spectra of 1-methyl-A_2, 2-methyl-A_2, 1,3-dimethyl-A_2 and 1-ethyl-A_2 with saturated chains, as well as 2-ethenyl-A_2 and 2-ethynyl-A_2 with unsaturated chains were measured using LIF technique. Then, the influences of these aliphatic branched chains on the fluorescence characteristics were analyzed base on the TD-DFT theoretical calculation.

3.2.1. Experimental results

The LIF spectra of six gas-phase PAHs with saturated and unsaturated aliphatic branched chains were shown in Fig. 6(a) and (b), respectively, in comparison with the spectrum of naphthalene. To show the variation of the spectrum shape, the LIF spectra of these gas-phase PAHs were normalized by their own maximum values. The normalization factors of the experimental LIF spectra of gas-phase PAHs in Fig. 6 were listed in Table 3, when the value of naphthalene is set as 1. The results showed that the spectrum of 2-methyl-A_2 was very coincident with the spectrum of A_2, indicating that the substituted methyl at 2-position of A_2 barely influenced the spectrum shape. Methyl at 1-position caused 2 nm redshifts of rising edge (at the half-maximum position, the same below) and 6 nm redshifts of falling edge, compared with the spectrum of A_2. When two methyls substituted the H atoms at 1-position and 3-position of A_2, the redshifts of the LIF spectrum were 3 nm and 9 nm at rising and falling edge respectively, which were larger than those of 1-methyl-A_2 and 2-methyl-A_2. By comparing the spectra of 1-methly-A_2 and 1-ethly-A_2, it can be concluded that the influences of the substituted methyl and ethyl at 1-position on the LIF spectrum of PAHs were almost identical. M. Orain et al. [73] measured the LIF spectra of A_2, 1-methyl-A_2 and 1,3-Dimethyl-A_2 at 450 K and 0.1 MPa, and their experimental findings were qualitatively accordance with the results presented in the current study.

Fig. 6(b) compared the LIF spectra of 2-ethenyl-A_2 and 2-ethynyl-A_2 with A_2, and the remarkable difference was displayed. When ethenyl and ethynyl substituted the hydrogen atom at 2-position of A_2, the LIF spectra shifted to the red and became broader, and the double-peak structures of A_2 spectrum also changed. For 2-ethenyl-A_2, the redshift of the rising edge and falling edge were 17 nm and 25 nm respectively, and for 2-ethynyl-A_2, the redshift of the rising edge and falling edge were 11 nm and 17 nm respectively. In summary, the saturated aliphatic branched chains (methyl and ethyl) only slightly influenced the LIF spectra, and in contrast, the unsaturated chains (ethenyl and ethynyl) caused more remarkable variations on the LIF spectra. Therefore, the influences of the aliphatic branched chains on PAH spectrum characteristics are important for the in-flame LIF measurement of PAHs, and the mechanism of these influences need to be further analyzed.

The evolutions of integral fluorescence intensities and normalized fluorescence spectra with temperatures in the range of 673−1373 K were presented in Figs. 7 and 8. The temperature dependences on the integral fluorescence intensities of 2-methyl-A_2

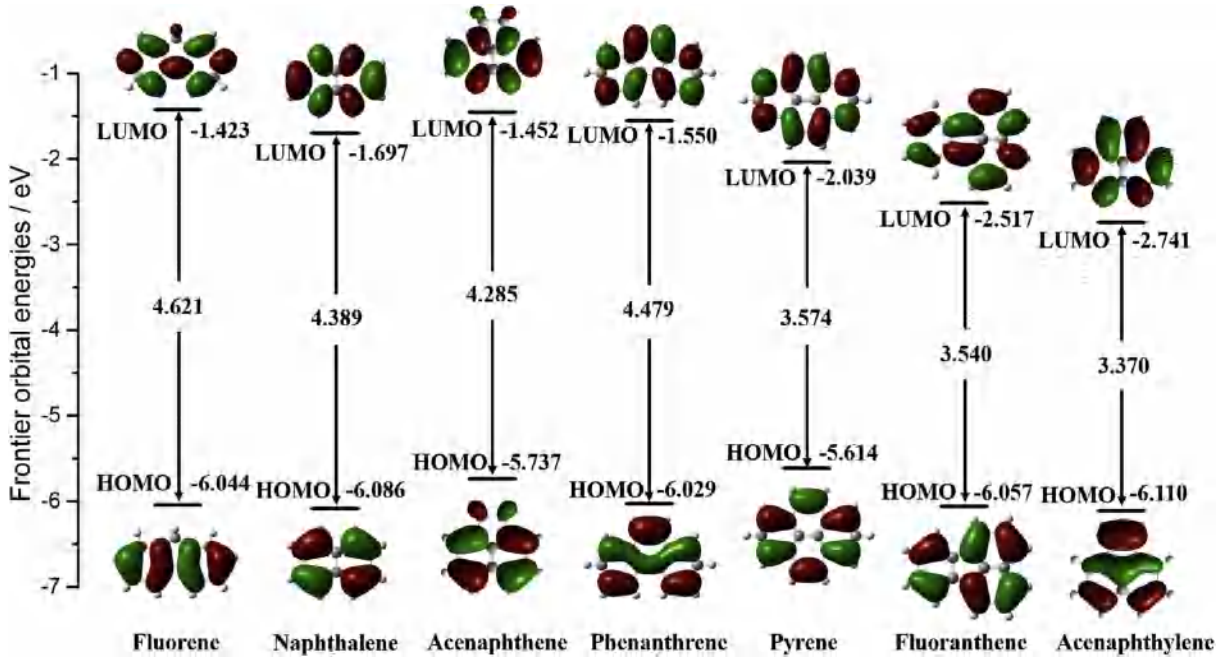

Fig. 5. The energy gaps (ΔE_{H-L}) between HOMO and LUMO and the electronic structures of HOMO and LUMO of seven gas-phase PAHs with different molecular size classes (The PAHs were listed in order of their fluorescence wavelengths).

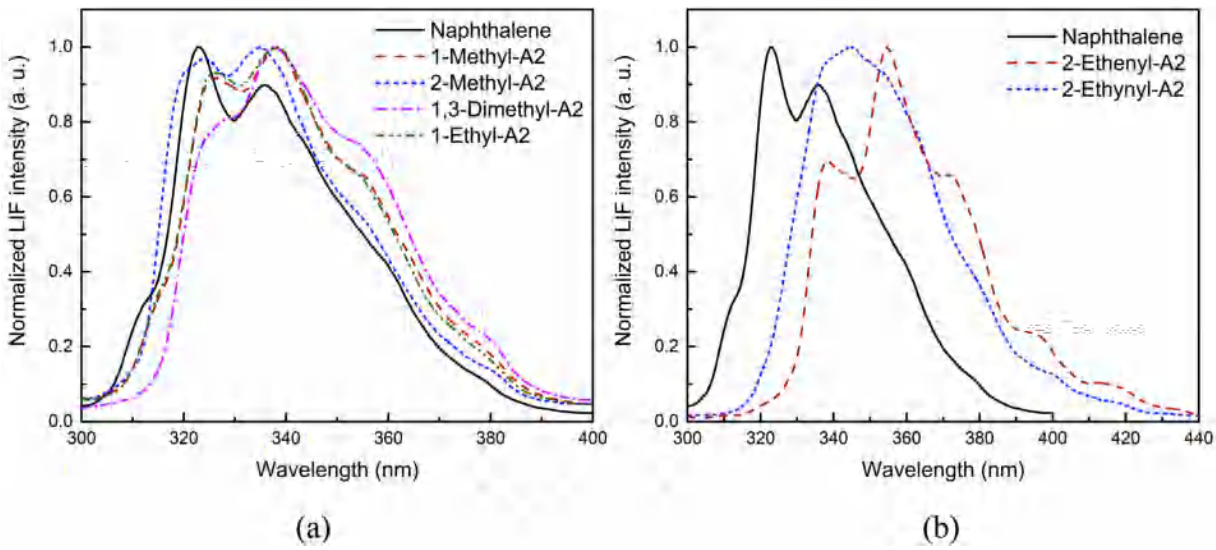

Fig. 6. Experimental LIF spectra of two-aromatic-ring PAHs with methyl, ethyl (a) and ethenyl, ethynyl (b) compared with the spectrum of naphthalene (A_2) at 673 K and 1 atm in argon.

and 2-ethynyl-A_2 were similar to that of A_2. While the descend magnitudes at the higher temperature are similar for 1-methyl-A_2, 1,3-dimethyl-A_2 and 1-ethyl-A_2 molecules, and were larger than that of A_2. The fluorescence intensities of 2-ethenyl-A_2 decreased sharply with increasing temperature and cannot be detected at temperatures higher than 1073 K. On the other hand, as shown in Fig. 8, the LIF spectra of all the PAHs with aliphatic branched chains shifted to the red and became broader as temperature increased.

3.2.2. Comparison of experimental and calculated LIF spectra

The experimental and calculated LIF spectra of 1-methyl-A_2, 1-ethyl-A_2, 2-ethenyl-A_2 and 2-ethynyl-A_2 were shown in Fig. 9. Unfortunately, the vibrationally-resolved electronic emission spectra of 2-methyl-A_2 and 1,3-dimethyl-A_2 cannot be calculated because the Franck-Condon factor corresponding to the overlap integral between both vibrational ground states is too small. This is an inherent limitation of Franck-Condon principle when the equilibrium geometry of the S_0 and S_1 are noticeably different and has been described in the literature [63]. Despite this limitation, the vertical emission energy, electron transition characteristics, and frontier molecular orbitals were obtained for subsequent analysis for 2-methyl-A_2 and 1,3-dimethyl-A_2. The experimental (black solid line) and calculated (red dashed line) LIF spectra shown in Fig. 9 indicated that TD-DFT calculation can well predict the experimental results.

3.2.3. Discussion based on the TD-DFT calculation

Based on the excellent performance of the TD-DFT calculation, the vertical emission energy of S_1 state and $S_0 \rightarrow S_1$ transition nature of six gas-phase PAHs with aliphatic branched chains were investigated, as listed in Table 4. The calculated results showed that the influences of the aliphatic branched chains at naphthalene on the vertical emission energy were well in accordance with the experimental result described in Section 3.2.1. The calculated transition natures showed that the $S_0 \rightarrow S_1$ transition was dominantly from the H → L transition for naphthalene and these PAHs with aliphatic branched chains.

Table 3
Normalization factors of the experimental LIF spectra of two-aromatic-ring PAHs with aliphatic branched chains.

Species	Naphthalene	1-methyl-A_2	2-methyl-A_2	1,3-dimethyl-A_2	1-ethyl-A_2
Factor	1	1.566	1.667	2.139	1.372
Species		2-ethenyl-A_2			2-ethynyl-A_2
Factor		0.807			1.320

In this section, the influences of the aliphatic branched chains on the electronic transition properties were analyzed based on the calculated frontier molecular orbitals, using the same method used in Section 3.1.3. The energy gaps (ΔE_{H-L}) between HOMO and LUMO and the electronic structures of HOMO and LUMO of these PAHs with aliphatic branched chains were calculated and compared with those of naphthalene, as shown in Fig. 10. The rank of the ΔE_{H-L} for these PAHs was identical with the rank of their experimental and calculated fluorescence wavelengths. The results further confirmed that the fluorescence emission wavelength ranges of PAHs can be accurately described by the energy gaps between HOMO and LUMO. The electronic structures of HOMO and LUMO of these PAHs were compared with that of naphthalene. The electron density plots of HOMO and LUMO showed that the saturated chains (methyl and ethyl) only slightly affected the electric structures of core aromatic rings while the unsaturated chains (ethenyl and ethynyl) significantly affected the electric structures of core aromatic rings. What's more, the double bond and triple bond

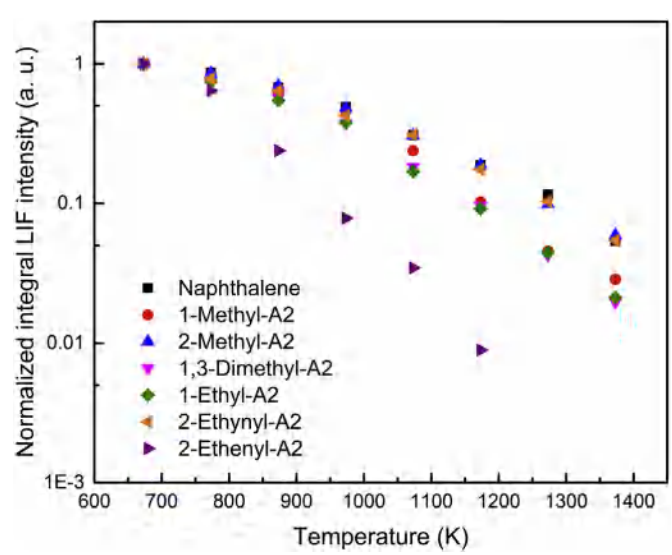

Fig. 7. Experimental integral intensities of naphthalene and six two-aromatic-ring PAHs with aliphatic branched chains in temperatures between 673 and 1373 K and 1 atm in argon.

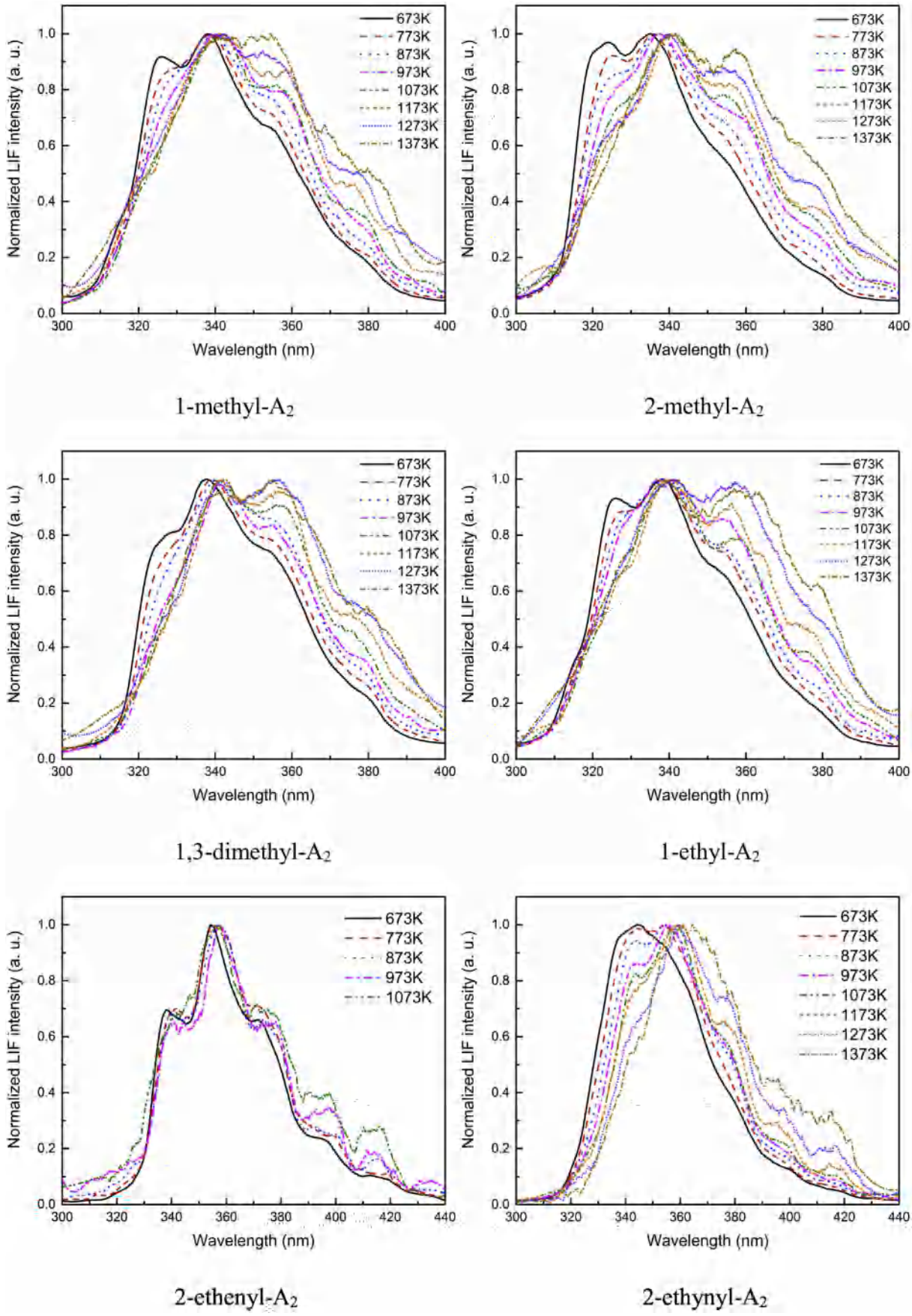

Fig. 8. Normalized experimental LIF spectra of six two-aromatic-ring PAHs with aliphatic branched chains in temperatures between 673 and 1373 K and 1 atm in argon.

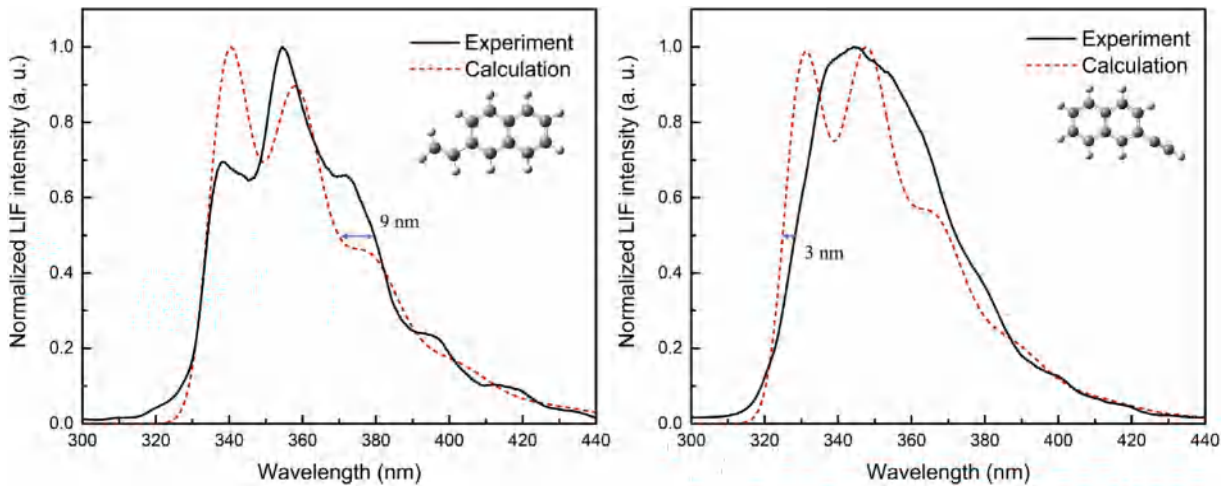

Fig. 9. Comparison of the experimental (black solid line) and calculated (red dashed line) LIF spectra of two-aromatic-ring PAHs with aliphatic branched chains.

of 2-ethenyl-A_2 and 2-ethynyl-A_2 also contributed to the H → L transition, extending the conjugated system of the original molecular structure, which was the key reason for longer emission wavelengths of 2-ethenyl-A_2 and 2-ethynyl-A_2 compared with that of naphthalene. In summary, the aliphatic branched chains will change ΔE_{H-L} by affecting the electric structures of HOMO and LUMO of the core aromatic rings, and then influence the fluorescence emission wavelength ranges.

Table 4
Electronic transition properties of six two-aromatic-ring PAHs with aliphatic branched chains compared with naphthalene (A_2).

Species	Vertical emission energy of S_1 state (eV, nm)	$S_0 \rightarrow S_1$ transition nature
Naphthalene	3.8227 (324.34)	H → L (96.8%)
1-methyl-A_2	3.7318 (332.24)	H → L (96.9%)
2-methyl-A_2	3.8161 (324.90)	H → L (95.6%)
1,3-dimethyl-A_2	3.7217 (333.14)	H → L (96.2%)
1-ethyl-A_2	3.7143 (333.81)	H → L (97.0%)
2-ethenyl-A_2	3.6356 (341.03)	H − 1 → L (7.7%) H → L (87.5%)
2-ethynyl-A_2	3.6543 (339.28)	H → L (96.1%)

4. Conclusion and outlooks

A systematic study was conducted to investigate fluorescence spectrum characteristics of 13 gas-phase PAHs with different molecular structures, including molecular size classes, five-membered ring structures, and aliphatic branched chains, using LIF measurement and TD-DFT calculation. The following conclusions can be remarked.

The experimental LIF spectra of naphthalene, phenanthrene, and pyrene indicated that the fluorescence emission wavelengths increased with more aromatic (benzenoid) rings. But when the PAH molecules contain the five-membered ring structures, the fluorescence emission wavelengths no longer show positive correlations

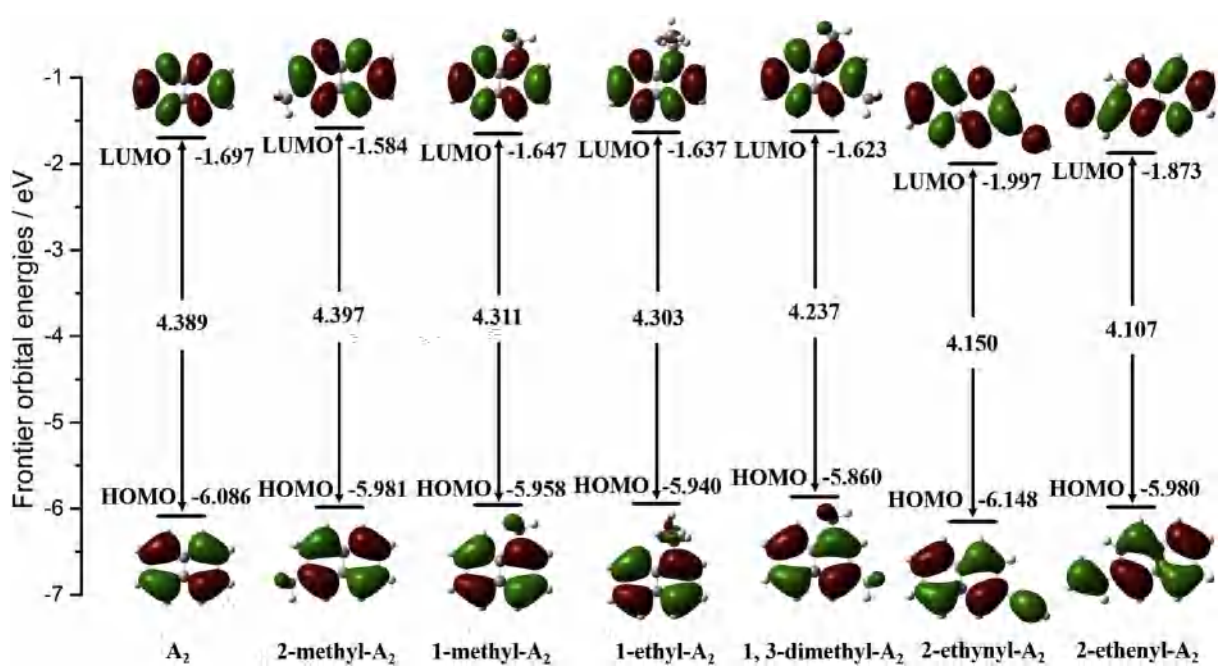

Fig. 10. The energy gaps (ΔE_{H-L}) between HOMO and LUMO and the electronic structures of HOMO and LUMO of naphthalene (A_2) and six two-aromatic-ring PAHs with aliphatic branched chains (The PAHs were listed in order of their fluorescence wavelengths).

with the molecular size classes. The calculated vibrationally-resolved emission spectra can well predict the measured LIF spectra. The electronic structures of HOMO and LUMO were significantly changed when PAH molecules have different molecular size classes and five-membered ring structures.

Then, we explored the influences of aliphatic branched chains substituted at naphthalene (A_2) on the fluorescence characteristics. The experiment results showed that the saturated aliphatic branched chains (methyl and ethyl) only slightly influenced the LIF spectra, while the unsaturated chains (ethenyl and ethynyl) caused more remarkable redshifts. The calculated emission spectra of these PAHs with aliphatic branched chains match well with the measured LIF spectra. The influences of the aliphatic branched chains were because the chains will change ΔE_{H-L} by affecting the electric structures of HOMO and LUMO of the core aromatic rings, and then influence the fluorescence emission wavelength ranges.

According to the analysis presented in this paper, it is extremely challenging to distinguish the relative size classes of PAHs in flames based on the fluorescence wavelength ranges, due to the complexity of the PAH molecular structures. In future works, the investigation of this kind of study should be extended to more PAHs which potentially exist in flames, in order to obtain more accurate information of PAHs in flames by LIF technique. In addition, for the species without pure standard substances, TD-DFT is a good method to predict their electronic emission spectra.

Acknowledgement

This work was funded by the National Natural Science Foundation of China (91441129, 51210010) and the National Key Research and Development Program of China (2016YFC0208000).

References

[1] J. Appel, H. Bockhorn, M. Frenklach, Kinetic modeling of soot formation with detailed chemistry and physics: laminar premixed flames of C2 hydrocarbons, Combustion and Flame 121 (2000) 122–136.
[2] H. Wang, M. Frenklach, A detailed kinetic modeling study of aromatics formation in laminar premixed acetylene and ethylene flames, Combustion and Flame 110 (1997) 173–221.
[3] P. Liu, Z. Li, A. Bennett, H. Lin, S.M. Sarathy, W.L. Roberts, The site effect on PAHs formation in HACA-based mass growth process, Combustion and Flame 199 (2019) 54–68.
[4] C.S. McEnally, L.D. Pfefferle, B. Atakan, K. Kohse-Höinghaus, Studies of aromatic hydrocarbon formation mechanisms in flames: Progress towards closing the fuel gap, Prog. Energy Combust. Sci. 32 (2006) 247–294.
[5] H. Liu, P. Zhang, X. Liu, B. Chen, C. Geng, B. Li, H. Wang, Z. Li, M. Yao, Laser diagnostics and chemical kinetic analysis of PAHs and soot in co-flow partially premixed flames using diesel surrogate and oxygenated additives of n-butanol and DMF, Combustion and Flame 188 (2018) 129–141.
[6] B. Chen, X. Liu, H. Liu, H. Wang, D.C. Kyritsis, M. Yao, Soot reduction effects of the addition of four butanol isomers on partially premixed flames of diesel surrogates, Combustion and Flame 177 (2017) 123–136.
[7] P. Liu, Z. Li, W.L. Roberts, The growth of PAHs and soot in the post-flame region, Proc. Combust. Inst. 37 (2019) 977–984.
[8] C.L. Friedman, Y. Zhang, N.E. Selin, Climate change and emissions impacts on atmospheric PAH transport to the Arctic, Environmental science & technology 48 (2013) 429–437.
[9] B. Binková, R.J. Šrám, The genotoxic effect of carcinogenic PAHs, their artificial and environmental mixtures (EOM) on human diploid lung fibroblasts, Mutation Research/Fundamental and Molecular Mechanisms of Mutagenesis 547 (2004) 109–121.
[10] W.M. Baird, L.A. Hooven, B. Mahadevan, Carcinogenic polycyclic aromatic hydrocarbon-DNA adducts and mechanism of action, Environ. Mol. Mutagen. 45 (2005) 106–114.
[11] P. Ehrenfreund, S.B. Charnley, Organic molecules in the interstellar medium, comets, and meteorites: a voyage from dark clouds to the early earth, Annu. Rev. Astron. Astrophys. 38 (2000) 427–483.
[12] J.Y. Seok, H. Hirashita, R.S. Asano, Formation history of polycyclic aromatic hydrocarbons in galaxies, Mon. Not. R. Astron. Soc. 439 (2014) 2186–2196.
[13] R. Rieger, K. Müllen, Forever young: polycyclic aromatic hydrocarbons as model cases for structural and optical studies, J. Phys. Org. Chem. 23 (2010) 315–325.
[14] S. Banerjee, D. Bhattacharyya, Electronic properties of nano-graphene sheets calculated using quantum chemical DFT, Comput. Mater. Sci. 44 (2008) 41–45.
[15] I. Glassman, Soot formation in combustion processes, Symp. Combust. 22 (1989) 295–311.
[16] H. Wang, Formation of nascent soot and other condensed-phase materials in flames, Proc. Combust. Inst. 33 (2011) 41–67.
[17] K. Johansson, J. Lai, S. Skeen, D. Popolan-Vaida, K. Wilson, N. Hansen, A. Violi, H. Michelsen, Soot precursor formation and limitations of the stabilomer grid, Proc. Combust. Inst. 35 (2015) 1819–1826.
[18] X. Mercier, O. Carrivain, C. Irimiea, A. Faccinetto, E. Therssen, Dimers of polycyclic aromatic hydrocarbons: the missing pieces in the soot formation process, Phys. Chem. Chem. Phys. 21 (2019) 8282–8294.
[19] Q. Wang, P. Elvati, D. Kim, K.O. Johansson, P.E. Schrader, H.A. Michelsen, A. Violi, Spatial dependence of the growth of polycyclic aromatic compounds in an ethylene counterflow flame, Carbon 149 (2019) 328–335.
[20] F. Bisetti, G. Blanquart, M.E. Mueller, H. Pitsch, On the formation and early evolution of soot in turbulent nonpremixed flames, Combustion and Flame 159 (2012) 317–335.
[21] D. Chen, H. Wang, HOMO-LUMO energy splitting in polycyclic aromatic hydrocarbons and their derivatives, Proc. Combust. Inst. 37 (2019) 953–959.
[22] F. Yan, L. Xu, Y. Wang, S. Park, S.M. Sarathy, S.H. Chung, On the opposing effects of methanol and ethanol addition on PAH and soot formation in ethylene counterflow diffusion flames, Combustion and Flame 202 (2019) 228–242.
[23] K. Kohse-Höinghaus, P. Oßwald, U. Struckmeier, T. Kasper, N. Hansen, C.A. Taatjes, J. Wang, T.A. Cool, S. Gon, P.R. Westmoreland, The influence of ethanol addition on premixed fuel-rich propene–oxygen–argon flames, Proc. Combust. Inst. 31 (2007) 1119–1127.
[24] P. Liu, Y. Zhang, Z. Li, A. Bennett, H. Lin, S.M. Sarathy, W.L. Roberts, Computational study of polycyclic aromatic hydrocarbons growth by vinylacetylene addition, Combustion and Flame 202 (2019) 276–291.
[25] Y. Wang, S.H. Chung, Soot formation in laminar counterflow flames, Prog. Energy Combust. Sci. 74 (2019) 152–238.
[26] K. Johansson, M. Head-Gordon, P. Schrader, K. Wilson, H. Michelsen, Resonance-stabilized hydrocarbon-radical chain reactions may explain soot inception and growth, Science 361 (2018) 997–1000.
[27] M. Thomson, T. Mitra, A radical approach to soot formation, Science 361 (2018) 978–979.
[28] B. Choi, S. Choi, S.-H. Chung, Soot formation characteristics of gasoline surrogate fuels in counterflow diffusion flames, Proc. Combust. Inst. 33 (2011) 609–616.
[29] S. Choi, B. Choi, S. Lee, J. Choi, The effect of liquid fuel doping on PAH and soot formation in counterflow ethylene diffusion flames, Exp. Thermal Fluid Sci. 60 (2015) 123–131.
[30] Y. Zhang, L. Wang, P. Liu, B. Guan, H. Ni, Z. Huang, H. Lin, Experimental and kinetic study of the effects of CO2 and H2O addition on PAH formation in laminar premixed C2H4/O2/Ar flames, Combustion and Flame 192 (2018) 439–451.
[31] P. Liu, Y. Zhang, L. Wang, B. Tian, B. Guan, D. Han, Z. Huang, H. Lin, Chemical mechanism of exhaust gas recirculation on polycyclic aromatic hydrocarbons formation based on laser-induced fluorescence measurement, Energy Fuel 32 (2018) 7112–7124.
[32] P. Zhang, H.-F. Liu, B.-L. Chen, Q.-L. Tang, M.-F. Yao, Fluorescence spectra of polycyclic aromatic hydrocarbons and soot concentration in partially premixed flames of diesel surrogate containing oxygenated additives, Acta Phys. -Chim. Sin. 31 (2015) 32–40.
[33] P. Desgroux, X. Mercier, K.A. Thomson, Study of the formation of soot and its precursors in flames using optical diagnostics, Proc. Combust. Inst. 34 (2013) 1713–1738.
[34] X. Mercier, A. Faccinetto, P. Desgroux, Laser Diagnostics for Selective and Quantitative Measurement of PAHs and Soot, Cleaner Combustion, Springer, 2013, pp. 303–331.
[35] F. Ossler, T. Metz, M. Aldén, Picosecond laser-induced fluorescence from gas-phase polycyclic aromatic hydrocarbons at elevated temperatures. I. Cell measurements, Applied Physics B 72 (2001) 465–478.
[36] F. Ossler, T. Metz, M. Aldén, Picosecond laser-induced fluorescence from gas-phase polycyclic aromatic hydrocarbons at elevated temperatures. II. Flame-seeding measurements, Applied Physics B 72 (2001) 479–489.
[37] Z. Chi, B.M. Cullum, D.L. Stokes, J. Mobley, G.H. Miller, M.R. Hajaligol, T. Vo-Dinh, High-temperature vapor detection of polycyclic aromatic hydrocarbon fluorescence, Fuel 80 (2001) 1819–1824.
[38] Z. Chi, B.M. Cullum, D.L. Stokes, J. Mobley, G.H. Miller, M.R. Hajaligol, T. Vo-Dinh, Laser-induced fluorescence studies of polycyclic aromatic hydrocarbons (PAH) vapors at high temperatures, Spectrochim. Acta A Mol. Biomol. Spectrosc. 57 (2001) 1377–1384.
[39] Y. Zhang, L. Wang, P. Liu, Y. Li, R. Zhan, Z. Huang, H. Lin, Measurement and extrapolation modeling of PAH laser-induced fluorescence spectra at elevated temperatures, Applied Physics B 125 (2019) 6.
[40] Y. Zhang, Y. Li, L. Wang, P. Liu, R. Zhan, Z. Huang, H. Lin, Investigation on the LIF spectrum superposition of gas-phase PAH mixtures at elevated temperatures: potential for the analysis of PAH LIF spectra in sooting flames, Applied Physics B 125 (2019) 72.
[41] P. Liu, H. Lin, Y. Yang, C. Shao, B. Guan, Z. Huang, Investigating the role of CH2 radicals in the HACA mechanism, J. Phys. Chem. A 119 (2015) 3261–3268.
[42] J.Y. Lai, P. Elvati, A. Violi, Stochastic atomistic simulation of polycyclic aromatic hydrocarbon growth in combustion, Phys. Chem. Chem. Phys. 16 (2014) 7969–7979.
[43] E.M. Adkins, J.H. Miller, Towards a taxonomy of topology for polynuclear aromatic hydrocarbons: linking electronic and molecular structure, Phys. Chem. Chem. Phys. 19 (2017) 28458–28469.
[44] S.-H. Chung, A. Violi, Peri-condensed aromatics with aliphatic chains as key intermediates for the nucleation of aromatic hydrocarbons, Proc. Combust. Inst. 33 (2011) 693–700.

[45] P. Elvati, A. Violi, Thermodynamics of poly-aromatic hydrocarbon clustering and the effects of substituted aliphatic chains, Proc. Combust. Inst. 34 (2013) 1837–1843.
[46] B. Shukla, M. Koshi, Comparative study on the growth mechanisms of PAHs, Combustion and Flame 158 (2011) 369–375.
[47] H. Jin, L. Xing, J. Hao, J. Yang, Y. Zhang, C. Cao, Y. Pan, A. Farooq, A chemical kinetic modeling study of indene pyrolysis, Combustion and Flame 206 (2019) 1–20.
[48] N. Hansen, M. Schenk, K. Moshammer, K. Kohse-Höinghaus, Investigating repetitive reaction pathways for the formation of polycyclic aromatic hydrocarbons in combustion processes, Combustion and Flame 180 (2017) 250–261.
[49] J.P. Cain, J. Camacho, D.J. Phares, H. Wang, A. Laskin, Evidence of aliphatics in nascent soot particles in premixed ethylene flames, Proc. Combust. Inst. 33 (2011) 533–540.
[50] J.P. Cain, P.L. Gassman, H. Wang, A. Laskin, Micro-FTIR study of soot chemical composition—Evidence of aliphatic hydrocarbons on nascent soot surfaces, Phys. Chem. Chem. Phys. 12 (2010) 5206–5218.
[51] D.L. Kokkin, N.J. Reilly, T.P. Troy, K. Nauta, T.W. Schmidt, Gas phase spectra of all-benzenoid polycyclic aromatic hydrocarbons: triphenylene, J. Chem. Phys. 126 (2007), 084304.
[52] J. Powell, E.C. Heider, A. Campiglia, J.K. Harper, Predicting accurate fluorescent spectra for high molecular weight polycyclic aromatic hydrocarbons using density functional theory, J. Mol. Spectrosc. 328 (2016) 37–45.
[53] P. Liu, Z. He, G.-L. Hou, B. Guan, H. Lin, Z. Huang, The diagnostics of laser-induced fluorescence (LIF) spectra of PAHs in flame with TD-DFT: special focus on five-membered ring, J. Phys. Chem. A 119 (2015) 13009–13017.
[54] S. Hirata, M. Head-Gordon, J. Szczepanski, M. Vala, Time-dependent density functional study of the electronic excited states of polycyclic aromatic hydrocarbon radical ions, J. Phys. Chem. A 107 (2003) 4940–4951.
[55] S. Hirata, T.J. Lee, M. Head-Gordon, Time-dependent density functional study on the electronic excitation energies of polycyclic aromatic hydrocarbon radical cations of naphthalene, anthracene, pyrene, and perylene, J. Chem. Phys. 111 (1999) 8904–8912.
[56] G. Malloci, C. Joblin, G. Mulas, On-line database of the spectral properties of polycyclic aromatic hydrocarbons, Chem. Phys. 332 (2007) 353–359.
[57] G. Malloci, G. Cappellini, G. Mulas, A. Mattoni, Electronic and optical properties of families of polycyclic aromatic hydrocarbons: a systematic (time-dependent) density functional theory study, Chem. Phys. 384 (2011) 19–27.
[58] J.-i. Aihara, Why are some polycyclic aromatic hydrocarbons extremely reactive? Phys. Chem. Chem. Phys. 1 (1999) 3193–3197.
[59] T.C. Allison, D.R. Burgess Jr, First-principles prediction of enthalpies of formation for polycyclic aromatic hydrocarbons and derivatives, J. Phys. Chem. A 119 (2015) 11329–11365.
[60] P. Klán, J. Wirz, Photochemistry of Organic Compounds: From Concepts to Practice, John Wiley & Sons, 2009.
[61] V. Barone, J. Bloino, M. Biczysko, F. Santoro, Fully integrated approach to compute vibrationally resolved optical spectra: from small molecules to macrosystems, J. Chem. Theory Comput. 5 (2009) 540–554.
[62] A.D. Becke, Density-functional thermochemistry. III. The role of exact exchange, J. Chem. Phys. 98 (1993) 5648–5652.
[63] V. Barone, J. Bloino, M. Biczysko, Vibrationally-Resolved Electronic Spectra in GAUSSIAN 09, Revision a vol. 2, 2009, pp. 1–20.
[64] J. Bloino, M. Biczysko, F. Santoro, V. Barone, General approach to compute vibrationally resolved one-photon electronic spectra, J. Chem. Theory Comput. 6 (2010) 1256–1274.
[65] M.J. Frisch, Gaussian09. http://www.gaussian.com/.
[66] F. Beretta, V. Cincotti, A. D'alessio, P. Menna, Ultraviolet and visible fluorescence in the fuel pyrolysis regions of gaseous diffusion flames, Combustion and flame 61 (1985) 211–218.
[67] A. Jurgensen, E. Inman Jr., J. Winefordner, Comprehensive analytical figures of merit for fluorimetry of polynuclear aromatic hydrocarbons, Anal. Chim. Acta 131 (1981) 187–194.
[68] B.F. Plummer, M. Hopkinson, J. Zoeller, Dual wavelength fluorescence from acenaphthylene and derivatives in fluid media, J. Am. Chem. Soc. 101 (1979) 6779–6781.
[69] A. Samanta, C. Devadoss, R.W. Fessenden, Picosecond time-resolved absorption and emission studies of the singlet excited states of acenaphthylene, J. Phys. Chem. 94 (1990) 7106–7110.
[70] S. Bejaoui, X. Mercier, P. Desgroux, E. Therssen, Laser induced fluorescence spectroscopy of aromatic species produced in atmospheric sooting flames using UV and visible excitation wavelengths, Combustion and Flame 161 (2014) 2479–2491.
[71] S. Premkumar, A. Jawahar, T. Mathavan, M.K. Dhas, V. Sathe, A.M.F. Benial, DFT calculation and vibrational spectroscopic studies of 2-(tert-butoxycarbonyl (Boc)-amino)-5-bromopyridine, Spectrochim. Acta A Mol. Biomol. Spectrosc. 129 (2014) 74–83.
[72] Y. Ruiz-Morales, HOMO– LUMO gap as an index of molecular size and structure for polycyclic aromatic hydrocarbons (PAHs) and asphaltenes: a theoretical study. I, J. Phys. Chem. A 106 (2002) 11283–11308.
[73] M. Orain, P. Baranger, B. Rossow, F. Grisch, Fluorescence spectroscopy of naphthalene at high temperatures and pressures: implications for fuel-concentration measurements, Applied Physics B 102 (2011) 163–172.